ACS Photonics

pubs.acs.org/journal/apchd5

Article

Light–Matter Interactions in Films of Randomly Distributed Unidirectionally Scattering Dielectric Nanoparticles

Parker R. Wray and Harry A. Atwater*

Cite This: https://dx.doi.org/10.1021/acsphotonics.0c00545

Read Online

ACCESS | Metrics & More | Article Recommendations | Supporting Information

ABSTRACT: We theoretically investigate the light scattering characteristics of monolayer films composed of randomly positioned unidirectionally scattering dielectric nanoparticles that support overlapping electric and magnetic dipole modes. We show using generalized Mie theory that the optical response of both sparse and dense nanoparticle films can be understood from the scattering properties of the individual dielectric nanoparticles, despite random particle–particle coupling effects and validate these results with full-wave electromagnetic simulations. The spectral, angular, and polarization dependent reflection and transmission scattering characteristics of these random particle films are also shown to be strikingly different from those of homogeneous dense solid thin films of equivalent dielectric permittivity.

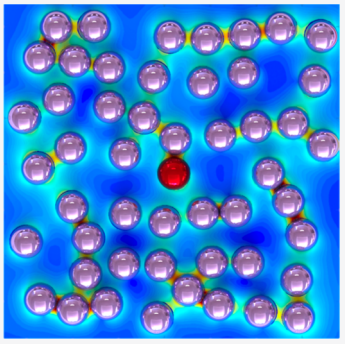

KEYWORDS: *Kerker scattering, random metamaterials, polarization invariance*

Scattering objects made of high index dielectrics offer the ability to generate low-loss electric and magnetic Mie resonances for light manipulation below the free-space diffraction limit.[1−7] Of notable interest, the addition of magnetic Mie resonances in spherical dielectric particles enables field distributions not achievable in metal counterparts, which support only resonant electric Mie modes.[4,5,8−10] This degree of freedom provides a compelling argument for the use of high index dielectrics in next generation metamaterial technologies. For example, overlapping electric and magnetic Mie modes have shown to produce dramatic unidirectional scattering, termed Kerker scattering.[5,9,11] Through precise particle placement, research in Kerker scattering particle films has shown new ways to design antireflective coatings, reflectors, absorbers, and other wavefront manipulating metasurfaces.[1,3,6−8,11−17] We expand on this growing body of research by studying the behavior of Kerker metasurfaces composed of randomly positioned but uniformly sized particles. We find the spectral, angular, and polarization response of these random Kerker metasurfaces to be dramatically distinct from dense solid thin films of equivalent dielectric permittivity. The particle films exhibit no polarization dependence and transmission and reflection peaks can be directly manipulated through proper design of the constituent particle. The results suggest that random films of Kerker particles could be used in designs of polarization invariant antireflective coatings or reflectors. Notably, random Kerker metasurfaces can be synthesized without the need for precise lithographic patterning, self-assembly, or layer stacking and thus could be fabricated using low-cost deposition methods such as plasma synthesis.

A scattering object with overlapping electric dipole (ED) and magnetic dipole (MD) modes and suppressed higher order modes will have a far-field scattering distribution that mimics an idealized point source (i.e., an only forward or backward propagating spherical wavelet) that is described by the Huygens-Fresnel principle.[18] Objects of this type are characterized by extreme forward-to-backward scattering ratios (FBR) dictated by the phase relationship between the ED and MD modes. They are also characterized by an even distribution in energy between the two modes, which gives rise to polarization invariance, meaning the scattering pattern looks the same in the direction parallel and perpendicular to the electric field.[11,19] The concept of overlapping electric and magnetic scattering modes was first introduced by Milton Kerker, in the context of elastic scattering from magnetic particles.[19] For this reason, the unique scattering behavior is often called Kerker scattering.

In recent years there has been rapidly expanding interest in Kerker scattering based on small dielectric particles. Though not magnetic, these particles support spectrally overlapping electric and magnetic dipole modes in the visible wavelength range. This is done by creating an optically induced magnetic resonance.[4,5,8−11,14,16,20−22] The use of Kerker particles in the

Received: April 5, 2020
Published: June 23, 2020

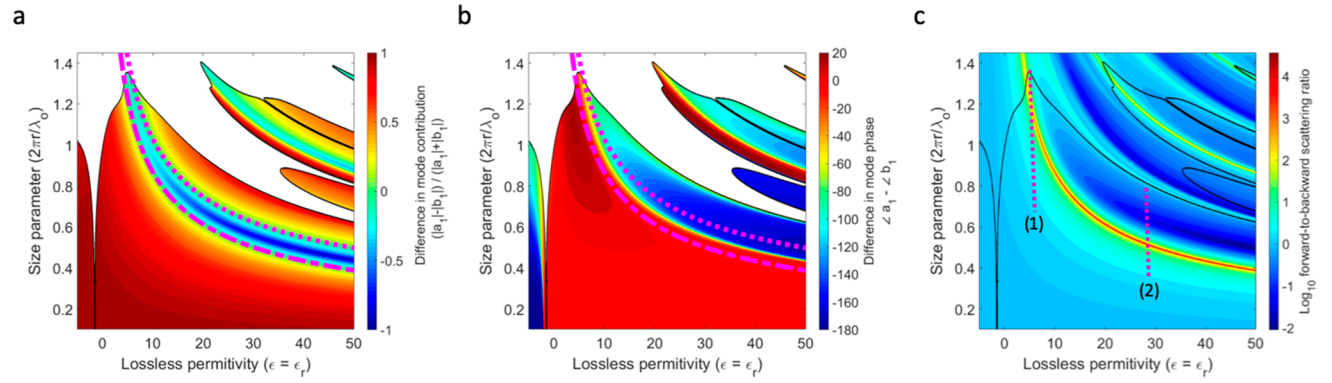

Figure 1. Parameter space for the single particle scattering coefficients showing the different Kerker regimes. (a) Normalized difference between the first order TM and TE scattering coefficients, as a function of size parameter and lossless permittivity. The dashed and dotted magenta line show the region where $\|a_1\|^2 = \|b_1\|^2$. The dashed line is under the dotted line. The white region is where the particle supports more than one mode, which is defined when the first order modes contribute less than 99% of the scattering cross-section. (b) The phase difference between the first order TM and TE mode. The dashed and dotted magenta lines are transferred from (a), to show the phase relationship in the regions where TM and TE mode energy is equal. The white region is also transferred from (a). (c) Log base 10 of the FBR which would occur from the magnitude and phase results in (a) and (b). The black outline denotes the transition region from single to multimode. Multimode regions are not overlaid with white. The first magenta dashed line shows and the forward-only scattering region. The second magenta line shows the region of backward-to-forward scattering transitions.

context of antenna arrays has been explored to produce highly directional scattering.[23] Previous research has shown that precise placement of Kerker particles in chains along the plane wave propagation direction can lead to a polarization-invariant scattered far field. Backward reflection could be substantially suppressed and forward directivity and side lobes could be tuned through particle spacing.[24] Particle clusters have been studied that were shown to collectively exhibit Kerker scattering behavior.[25−27] Random silicon trimer and quadrimer particle clusters in different orientations were shown to behave like effective Kerker particles.[27] The magnetic response was attributed to the individual nanoparticle, whereas the electric component was attributed to gap modes between particles.[27] Films composed of Kerker particles have also been studied in 2D and 3D ordered periodic arrays. Lattices of various types have been studied in the metasurface regime, where the subwavelength periodicity produces no diffraction orders, and in the grating regime, where diffraction is present at various orders.[2829] This body of work has led to the theoretical predictions and experimental verification of near perfect transmission,[30,31] reflection,[32,33] and absorption[16,34] in ordered arrays, through particle design and lattice spacing.

In this paper, we show that 2D films of randomly placed Kerker particles also give rise to behavior that cannot be replicated by equivalent homogeneous dense thin film analogs. The key finding is that, in an average sense, nanoparticles will retain their Kerker behavior in the presence of random interparticle coupling. This occurs despite the stringent requirement placed on both the amplitude and phase of the ED and MD modes. The result is that the optical properties of both sparse and dense monolayer films of randomly distributed Kerker particles can be accurately predicted from the scattering characteristics of single particle building blocks. The specular, angular, and polarization dependent properties are distinctly different from dense homogeneous thin film analogs. Our analysis uses generalized Mie theory, which completely accounts for particle coupling. This framework creates satisfying parallels between studying random Kerker particle films and the use of traditional Mie theory for the design of isolated Kerker particles.

DESIGN OF ED/MD OVERLAPPING KERKER PARTICLES

The phenomenon of Kerker scattering from a spherical particle can be directly seen from Mie theory.[35] In the far field limit, the amplitude response of elastic scattering from a wave incident on a particle can be written in a convenient matrix form

$$\begin{bmatrix} E_s^{\parallel} \\ E_s^{\perp} \end{bmatrix} = \frac{e^{ikR}}{-ikR} \begin{bmatrix} S_2 & S_3 \\ S_4 & S_1 \end{bmatrix} \begin{bmatrix} E_i^{\parallel} \\ E_i^{\perp} \end{bmatrix} \tag{1}$$

where E_s is the elastic scattered electric field amplitude, E_i is the incident field amplitude, $\parallel$ and $\perp$ represent the planes parallel and perpendicular to the scattering plane,[35] k is the wavenumber in the surrounding media, and R is the radial observation distance from the particle's origin. S_j $(j = 1{-}4)$ is the element of the amplitude scattering matrix. For a single particle under plane wave illumination, there is no polarization conversion $(S_3 = S_4 = 0)$.[35] If all scattering coefficients beyond the first order are negligible, the angle-resolved far field scattering efficiency parallel, $Q_s^{\parallel}(\theta)$, and perpendicular, $Q_s^{\perp}(\theta)$, to the scattering plane are given by

$$Q_s^{\parallel}(\theta) = \frac{S_2^{\,2}}{x^2} = \frac{1}{x^2}(a_1^{\,2}\tau_1^2 + b_1^{\,2}\pi_1^2 + (a_1 b_1^* + b_1 a_1^*)\pi_1\tau_1) \tag{2}$$

and

$$Q_s^{\perp}(\theta) = \frac{S_1^{\,2}}{x^2} = \frac{1}{x^2}(b_1^{\,2}\tau_1^2 + a_1^{\,2}\pi_1^2 + (a_1 b_1^* + b_1 a_1^*)\pi_1\tau_1) \tag{3}$$

where $\tau_n = \frac{dP_n^1(\cos(\theta))}{d\theta}$ and $\pi_n = \frac{P_n^1(\cos(\theta))}{\sin\theta}$ are the angle-dependent basis functions, based on the associated Legendre polynomial (P_n^m) of order n and degree $m = 1$. The coefficients for this basis are a_n for transverse magnetic (TM) modes and b_n for transverse electric (TE) modes. These coefficients are found by applying the boundary conditions of field continuity between the particle and environment, leading to the well-

https://dx.doi.org/10.1021/acsphotonics.0c00545
ACS Photonics XXXX, XXX, XXX−XXX

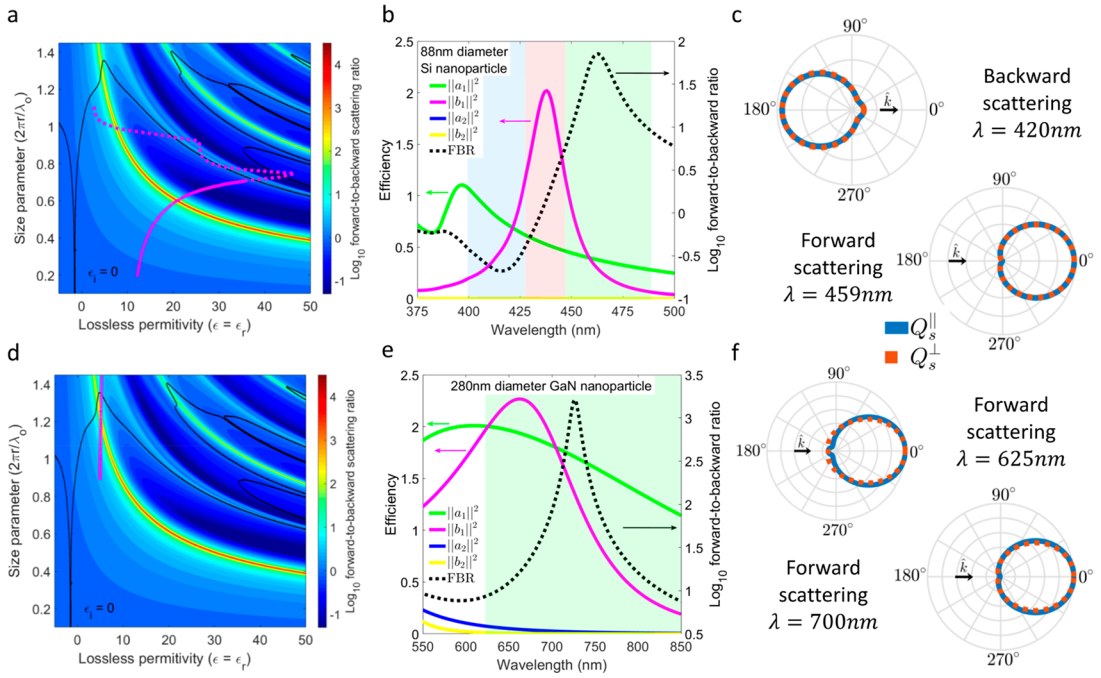

Figure 2. Scattering profiles of a 88 nm diameter Si particle and a 280 nm diameter GaN particle. (a) The log base 10 FBR from Figure 1c, with the permittivity of silicon overlaid in magenta, as a function of size parameter (x = 2π44 [nm]/λ_o [nm]). The dashed magenta line represents the region of Si permittivity that is not applicable for the graph, due to material loss. The solid magenta line is the region of Si applicable to the graph (ϵ_i < 0.7). (b) Efficiency scaled magnitude response of the dominant scattering coefficients in the Si particle's scattering cross-section (solid lines). The dashed black line plots the log base 10 FBR of the Si particle, as a function of wavelength, in the regions showing the backward scattering (blue), the optically induced artificial magnetic resonance (red), and the forward scattering (green) regime. (c) The angle-resolved far field scattering profiles near the backward and forward Kerker resonances in the Si particle. (d−f) The analogous graphs from (a)−(c) for a 280 nm diameter GaN particle. For 280 nm diameter GaN, only forward-dominant scattering is present and second order modes become appreciable at shorter wavelengths (λ < 650 nm). All magnitude responses are efficiency scaled based on the formula $\frac{2}{x^2}(2n+1)\delta_n^2$, where $\delta_n = a_n$ or b_n and n is the mode order.

known Mie solutions.[35] The asterisk over the variable denotes the complex conjugate and the n = 1 subscript represent the dipole modes. The argument $x = \frac{2\pi r}{\lambda_0}$, called the size parameter, is a unitless ratio between the particle radius (r) and the free-space wavelength (λ_0). In the forward (θ = 0°) and backward (θ = 180°) scattering directions, the parallel and perpendicular scattering efficiencies are the same. Therefore, the forward-to-backward ratio (FBR) is defined as FBR = $Q_s(\theta = 0°)/Q_s(\theta = 180°)$, where either $Q_s^{\parallel}(\theta)$ or $Q_s^{\perp}(\theta)$ can be used.

Kerker's condition for forward scattering requires $a_1 = b_1$ and backward scattering requires $a_1 = -b_1$.[19] The condition $\|a_1\|^2 = \|b_1\|^2$ creates polarization invariance. Therefore, Kerker scattering requires an even distribution of energy between the transverse electric (TE) and transverse magnetic (TM) modes, while the propagation direction is directly related to the relative phase of the coefficients due to the interference term. Figure 1 depicts the entire particle size-permittivity parameter space, where the Kerker conditions are satisfied for the first order (dipole) case. The contribution of higher order modes is shown in Figure S1. The plots assume a particle with lossless permittivity ($\epsilon = \epsilon_r$) and unity relative permeability (μ_r = 1) with a background of free space. The assumption of negligible loss is justified in Figure S2. Figure 1a shows the difference in energy distribution between the first order TE and TM modes. The dotted and dashed magenta lines indicate where the TE and TM mode energies are equal. Figure 1b shows the relative phase between these two modes. From the phase profile we see the dashed magenta line corresponds to the forward Kerker condition, whereas the dotted magenta line is approaching the backward Kerker condition with increasing permittivity. Between these two regions is an optically induced artificial magnetic resonance.[8] Figure 1c shows the resulting FBR that would be achieved as a result of the magnitude and phase relationships from Figure 1a,b. This figure shows that there are two distinct Kerker regimes for real passive materials: (1) a region where forward-scattering is always dominant and (2) a region producing a backward-to-forward scattering transition.

As an example of Kerker scattering for passive materials, Figure 2 shows the response of an 88 nm diameter silicon (Si[36]) particle illustrating the backward-to-forward scattering regime, and a 280 nm diameter gallium nitride (GaN[37]) particle, as an example of the forward-only scattering regime. For the 88 nm diameter Si particle, the wavelength range from 400 to 500 nm is sufficient to study backward-to-forward scattering. In the case of the 280 nm diameter GaN particle, we find forward-only scattering with optimal forward scattering from 675 to 800 nm. We find wavelength ranges from 550 to 600 nm are shown to have appreciable second order terms. This region is not considered in our analysis, despite maintaining forward dominant scattering, since we are primarily interested in overlapping ED and MD modes. All calculations for Figures 1 and 2 were done using a Mie theory scattering formalism.[38]

https://dx.doi.org/10.1021/acsphotonics.0c00545
ACS Photonics XXXX, XXX, XXX−XXX

EFFECT OF RANDOMLY DISTRIBUTED NANOPARTICLE COUPLING

As described in the previous sections, Kerker scattering requires a particle to satisfy stringent magnitude and phase relationships between modes. To study the effect of random nanoparticle coupling, we generate random monolayer films of same sized Kerker particles and calculate how interparticle coupling alters the scattering behavior of an individual particle within the film. This is done using the generalized Mie theory, which is a complete analytical solution to the problem of multiple scattering and interparticle coupling between particles.[39,40] Interestingly, we find that the average response will continue to satisfy Kerker's stringent amplitude and phase conditions. This is true even when the average nearest neighbor distance is well within the near field coupling regime. We then show, in the next section, that this average response has a direct relationship to the scattering behavior of an infinite randomly distributed particle film.

When dealing with coupled nanoparticles, polarization conversion can occur. Since this property is not seen in isolated Mie theory, it is necessary to work with the full scattering matrix from eq 1 to define a particle's scattering response. The particle's angle resolved scattering efficiency is written in the general form

$$Q_s^{\parallel}(\theta) = \frac{1}{x^2}({S_2}^2 + {S_3}^2 + S_2S_3^* + S_2^*S_3) \tag{4}$$

and

$$Q_s^{\perp}(\theta) = \frac{1}{x^2}({S_4}^2 + {S_1}^2 + S_4S_1^* + S_4^*S_1) \tag{5}$$

Furthermore, in generalized Mie theory it cannot be assumed that degree (m) in the modal expansion is unitary. Therefore, the scattering amplitude elements (S_1−S_4) are fully expanded with respect to degree (m), order (n), and mode (TE or TM). The derivation for converting the scattering amplitude elements from isolated Mie theory to generalized Mie theory is presented in section 2 of the Supporting Information.

Using the generalized framework, we simulate finite-sized random monolayer nanoparticle films with 10%, 20%, 30%, and 40% area fill fraction. The packing densities correspond to an average nearest neighbor distance ranging from 68 to 10 nm. Gap distances as small as zero (i.e., touching particles) are allowed and do occur. Simulations are done for both 88 nm diameter Si and 280 nm diameter GaN particles, to study both the forward-to-backward and forward-only Kerker scattering regimes. The method emulates simulating a particle in an infinite film by deterministically placing an "observation particle" at the origin, then generating a sufficiently large number of particles surrounding it. The surrounding particles are placed based on a uniform distribution (i.e., equal probably of finding a particle at any location where particles do not overlap) around the observation particle. The spatial autocorrelation of these random particle distributions is shown in Figure S3 for Si and Figure S4 for GaN. The generalized Mie program is then run on each finite particle film and the resulting scattering coefficients for the observation particle is recorded, accounting for all interparticle coupling. This process is repeated for 50 unique particle distributions, simulating both parallel and perpendicular incident polarization at normal incidence (100 simulations in total). Repeating the simulation procedure on unique distributions is designed to mimic randomly sampling particles in an infinite film.

In both the loose and densely packed cases, we find the average response of the observation particle is weakly affected by coupling between surrounding particles. The effect of particle coupling became more pronounced as fill fraction increased. Though, on average, the resulting spectral profile exhibits the same type of Kerker scattering as is seen for isolated particles. We find that particle coupling does not excite higher order modes within the Kerker particles, as all scattering coefficients having orders greater than one ($n > 1$) were shown to be negligible (detail for 88 nm diameter Si particles is shown in Figure S5 and for 280 nm diameter GaN particles in Figure S6). Therefore, we need only consider $mn = \{11,-11\}$. Unlike the isolated Mie solution, in both Si and GaN, polarization conversion was present. For the scattering coefficients associated with polarization conversion, their phase profiles mimicked a uniform distribution. Their magnitudes mimicked the parallel-to-parallel or perpendicular-to-perpendicular coefficients with, on average, an order of magnitude less strength (detail for 88 nm diameter Si particles is shown in Figure S5 and for 280 nm diameter GaN particles in Figure S6). In other words, the polarization conversion scattering elements, S_3 and S_4, had random phase. They also had magnitudes that were 1 order of magnitude less than S_1 and S_2 and have similar spectral shape. This result simplifies eqs 4 and 5, with respect to the average response since $E[S_2S_3^* + S_2^*S_3] \approx E[S_4S_1^* + S_4^*S_1] \approx 0$. We can intuit the random phase of the polarization converted field from the fact that this field is a direct result of the scattered field from the surrounding particles impinging on the observation particle. Since these particles are a random distance from the observation particle, their phase profiles do not coherently overlap.

In general, particle clusters are not rotationally symmetric, so scattering coefficients for parallel and perpendicular incident polarization are different. We can intuitively understand this lack of symmetry by considering particle dimers. In dimers, the electric field distribution can be different depending on if particles are aligned on or off axis with respect to the incident polarization. For an infinite film we can remove this polarization dependence, with respect to the average response, by including particle distributions rotated by 90° when performing the average.

Removing the negligible higher order terms and incorporating all relevant simplifications discussed above, the average angle-resolved scattering efficiency for a particle in a randomly positioned Kerker film can be simplified to

$$E[Q_s^{\parallel}(\theta)] = \frac{1}{x^2}E\begin{bmatrix}(\|A_{11}\|^2 + \|A_{11}^{\times}\|^2)\tau_{11}^2 \\ + (\|B_{11}\|^2 + \|B_{11}^{\times}\|^2)\pi_{11}^2 \\ + (A_{11}B_{11}^* + A_{11,}^*B_{11})\tau_{11}\pi_{11}\end{bmatrix} \tag{6}$$

and

$$E[Q_s^{\perp}(\theta)] = \frac{1}{x^2}E\begin{bmatrix}(\|B_{11}\|^2 + \|B_{11}^{\times}\|^2)\tau_{11}^2 \\ + (\|A_{11}\|^2 + \|A_{11}^{\times}\|^2)\pi_{11}^2 \\ +(A_{11}B_{11}^* + A_{11}^*B_{11})\tau_{11}\pi_{11}\end{bmatrix} \tag{7}$$

The variables A_{mn} and B_{mn} are the TM and TE modes associated with energy transfer between same polarization

https://dx.doi.org/10.1021/acsphotonics.0c00545
ACS Photonics XXXX, XXX, XXX−XXX

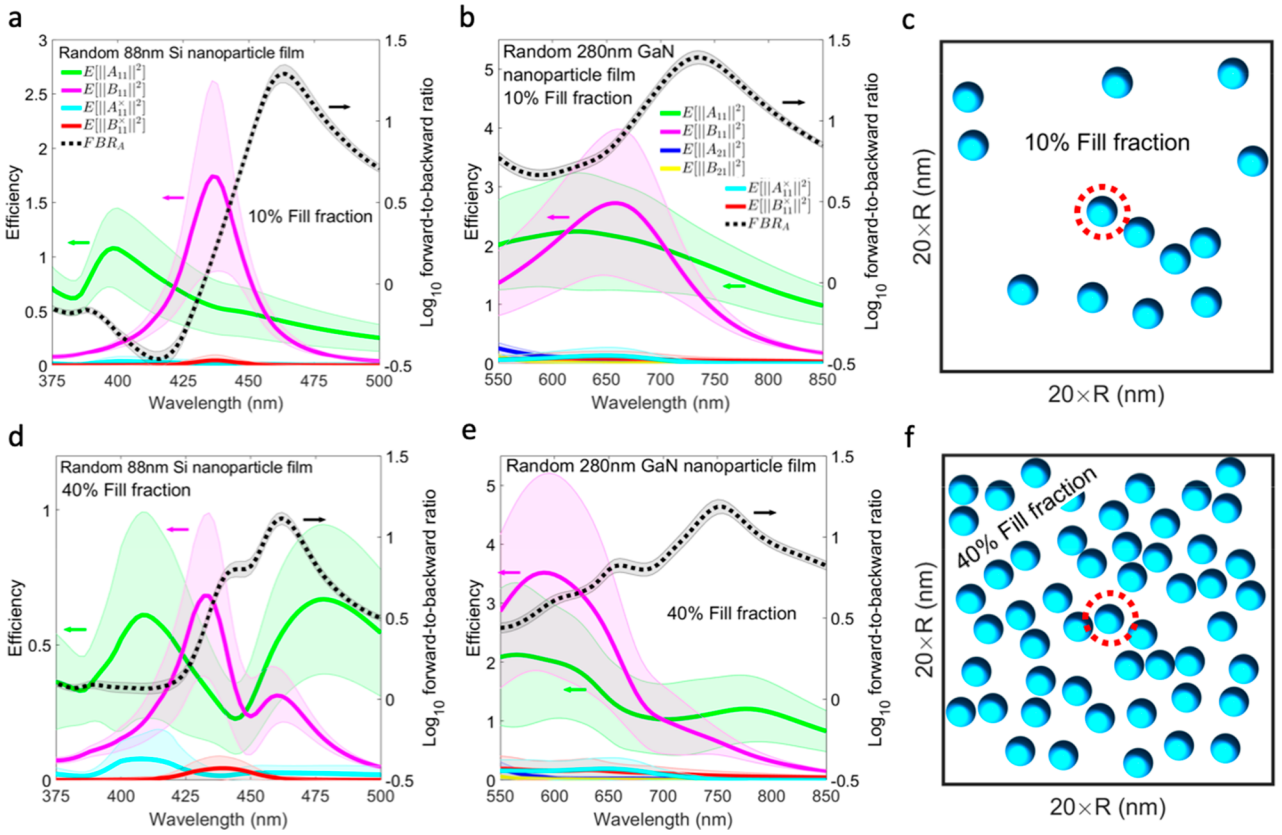

Figure 3. Scattering behavior of Kerker particles embedded in a random monolayer Kerker particle film. (a, d) Efficiency scaled magnitude of the dominant scattering modes and FBR_A for an 88 nm diameter Si particle embedded in a random particle film with fill fractions of (a) 10% and (d) 40%. (b, e) Corresponding results for a 280 nm diameter GaN particle embedded in a random particle film with fill fractions of (b) 10% and (e) 40%. (c, f) Top-view graphical representation of a random particle film with fill fractions of (c) 10% and (f) 40%. The red dashed circle outlines the observation particle. The length and width of the film are given as a function of particle radius (R). The solid color lines show the average (N = 100) mode contribution to the independent scattering efficiency (left y-axis). The dashed black line shows the FBR_A for the average scattering response (right y-axis). The corresponding shaded areas is the area one standard deviation from the mean. All magnitude responses are efficiency scaled based on the formula $\frac{2}{x^2}E[\Delta_{nm}{}^2]$, where $\Delta = A, B, A^{\times}$, or $B^{\times}$.

states. The variables $A^{\times}_{mn}$ and $B^{\times}_{mn}$ account for cross-polarization energy transfer. Averaging is taken over observation particles, including sets of 90° rotations. The derivation of eqs 6 and 7 are provided in section 2 of the Supporting Information.

Equations 6 and 7 show a surprising result. A first-order Kerker particle's average scattering response function in a random film is nearly identical to its isolated scattering response function shown in eqs 2 and 3. The difference is only in the addition of first-order incoherent polarization conversion terms. Consequently, the FBR of the average scattering response can be written in a similar form to the isolated Mie case, as $\mathrm{FBR}_A = \frac{E[Q_s(\theta = 0°)]}{E[Q_s(\theta = 180°)]}$. Either $E[Q_s^{\parallel}(\theta)]$ or $E[Q_s^{\perp}(\theta)]$ can be used as long as we are considering all sets accounting for 90-degree rotations. Justification for the definition of the FBR_A is provided in section 4 of the Supporting Information. For randomly distributed Kerker particles, the phase relationship that determines forward or backward Kerker scattering is given by only the primary first order modes, $E[A_{11}\, B_{11}^{*} + A_{11}^{*}\, B_{11}]$. Therefore, for both forward and backward Kerker scattering, it is necessary that $E[\|A_{11}\|^2] = E[\|B_{11}\|^2]$ and that $E[\|A_{11}^{\times}\|^2]$ and $E[\|B_{11}^{\times}\|^2]$ approach zero, since the cross-polarization coefficients are not present in the interference term. The condition of polarization invariance is generalized to $E[\|A_{11}\|^2 + \|A_{11}^{\times}\|^2] = E[\|B_{11}\|^2 + \|B_{11}^{\times}\|^2]$, indicating that it is not necessary for cross-polarization terms to vanish in order to satisfy polarization invariance.

Figure 3 shows the average magnitude response of the prominent scattering coefficients found in a randomly coupled Kerker particle as well as the particle's FBR_A. The results are shown for 88 nm diameter Si nanoparticle films with (a) 10% and (d) 40% fill fraction and for 280 nm diameter GaN nanoparticle films with (b) 10% and (e) 40% fill fraction. Results for 20% and 30% fill fraction are shown in Figure S7. We see, for nanoparticles in both the forward-only and backward-to-forward Kerker scattering regimes (280 nm diameter GaN and 88 nm diameter Si, respectively), the average scattering coefficients mimic the overall shape of the mode profiles for the isolated Mie solution from Figure 2. Furthermore, the FBR_A for the coupled and isolated case follow a similar profile, indicating correct phase behavior. The phase response of the primary scattering coefficients is presented in Figure S5 for 88 nm diameter Si and Figure S6 for 280 nm diameter GaN. From the results above we find that a Kerker particle embedded in a random monolayer film of Kerker particles will retain the Kerker scattering behavior of its isolated particle solution, in an average sense, despite the effects of random particle coupling. All FBR_As were calculated using the general formulas from eqs 4 and 5, assuming no simplifications, to validate eqs 6 and 7. In Figure 3, the mode

https://dx.doi.org/10.1021/acsphotonics.0c00545
ACS Photonics XXXX, XXX, XXX−XXX

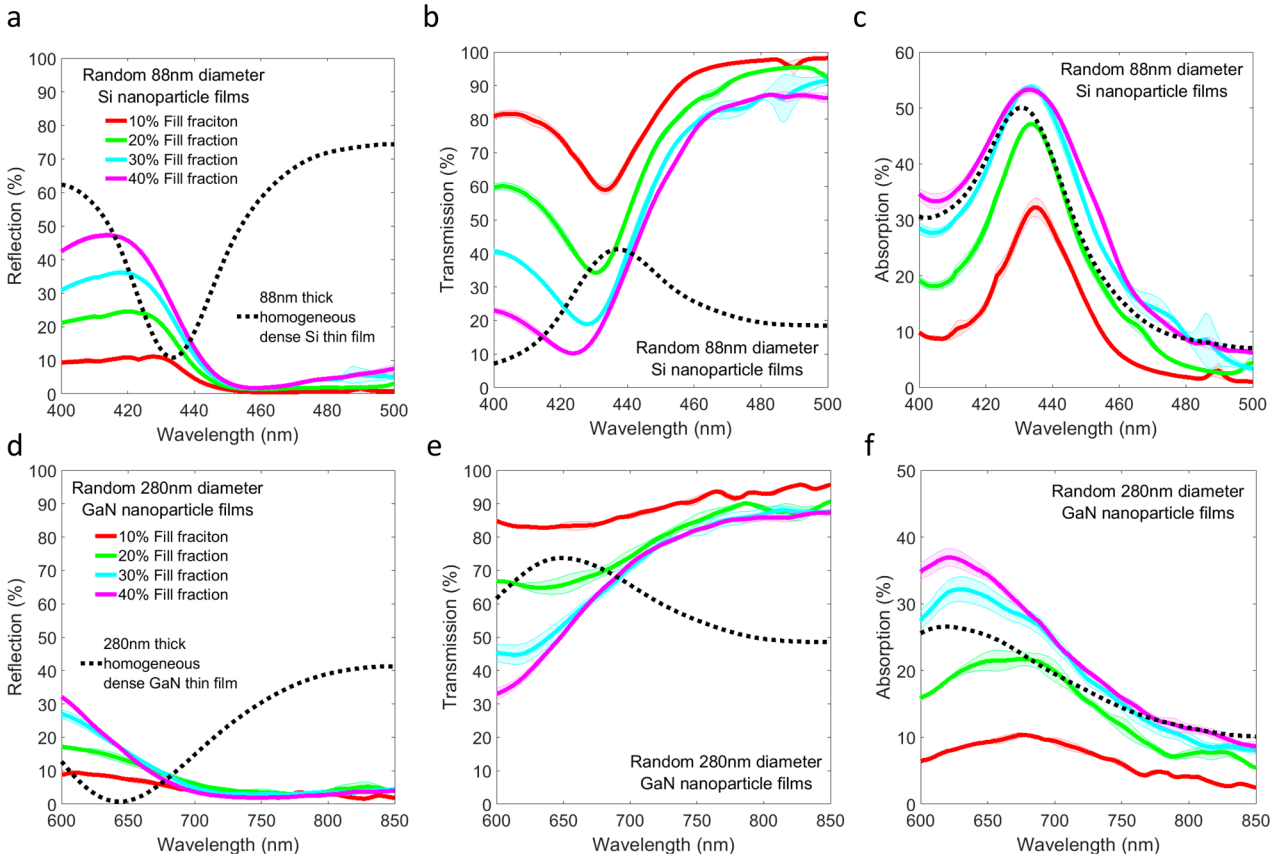

Figure 4. Reflection, transmission, and absorption of random nanoparticle films made of Kerker particles, calculated using FDTD. (a−c) RTA of random particle films made of 88 nm diameter Si particles for area fill fractions ranging from 10 to 40%. The colored solid lines represent the average response over three simulations of distinct random distributions. The colored shaded region represents the area within one standard deviation of the mean. The dashed black line shows the RTA for an 88 nm thick dense homogeneous thin film slab of Si. (d−f) Corresponding results for random particle films of 280 nm diameter GaN particles. The dashed black like shows the corresponding response for a 280 nm thick dense homogeneous thin film slab of GaN.

decomposed independent scattering efficiencies are defined as $\frac{2}{x^2}E[\|\Delta_{nm}\|^2]$, where $\Delta = A, B, A^{\times}$, or $B^{\times}$. These mode decomposed efficiencies will sum to the independent particle's scattering efficiency. This is not the same as the total scattering efficiency due to the interference effect between particles. More information about particle efficiencies under the generalized Mie theory framework is presented in section 3 of the Supporting Information.

MONOLAYER FILMS OF RANDOMLY DISTRIBUTED KERKER PARTICLES

To corroborate our results from generalized Mie theory and further study the reflection, transmission, absorption (RTA), and polarization-dependent behavior of these films, we simulate the random nanoparticle films using full-wave finite-difference time-domain (FDTD) simulations.[41]

Random nanoparticle films with length and width dimensions of 40× the particle radius was repeated using Bloch boundary conditions to model an infinite random structure. Figure 4a−c shows the RTA behavior of 88 nm diameter Si random nanoparticle films in the backward-to-forward Kerker regime. Area fill fractions ranged from 10 to 40% and illumination was normal incidence. Figure 4d−f shows the corresponding RTA results for 280 nm diameter GaN random films in the forward-only regime. In all cases, three distinct random particle distributions were simulated using FDTD. The solid lines are the average from the three distinct simulations. The shaded region represents the area within one standard deviation of the average. In all cases, the reflection and transmission properties of these films were dramatically different from the behavior of a corresponding homogeneous dense thin film. The RTA response of a homogeneous dense thin film with a thickness equal to the corresponding nanoparticle diameter is given by the dashed black line.

We find the dominant scattering feature in these films is similar to that of an isolated nanoparticle building block. To highlight this, we propose the formula

$$R = \frac{ffE[\sigma_{sca}]}{1 + FBR}, \quad A = ffE[\sigma_{abs}], \quad T = 1 - A - R \tag{8}$$

which estimates the film's spectral reflection (R), absorption (A), and transmission (T) response based only on parameters from the average Kerker particle scattering behavior and the particle film's area fill fraction (ff). The FBR_A, average observation particle scattering efficiency ($E[\sigma_{sca}]$), and average observation particle absorption efficiency ($E[\sigma_{abs}]$) are calculated from the simulations performed in section three. The scattering efficiency is determined through the equation

$$E[\sigma_{ext}] - E[\sigma_{abs}] = E[\sigma_{sca-i}] + E[\sigma_{sca-d}] = E[\sigma_{sca}] \tag{9}$$

https://dx.doi.org/10.1021/acsphotonics.0c00545
ACS Photonics XXXX, XXX, XXX−XXX

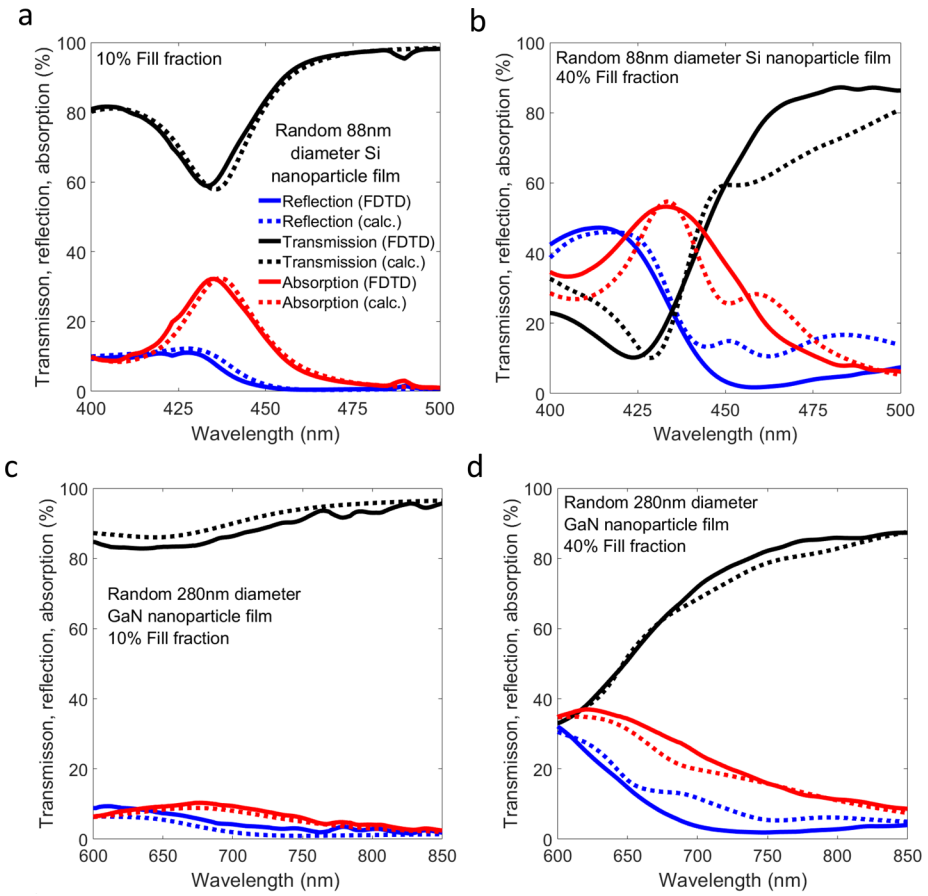

Figure 5. Comparison of the reflection, transmission, and absorption in random monolayer Kerker films at normal incidence. In all cases the solid lines are the average FDTD-based RTA response, taken from Figure 4, and the dashed lines are the average RTA response predicted from eq 8 using the data from section 2. (a, b) RTA of 88 nm diameter Si random particle films for (a) 10% and (b) 40% fill fraction. (c, d) RTA of the 280 nm diameter GaN random particle films for (c) 10% and (d) 40% fill fraction.

where $\sigma_{ext,j}$ is the extinction efficiency, $\sigma_{abs,j}$ is the absorption efficiency, $\sigma_{sca\text{-}i,j}$ is the independent scattering efficiency, and $\sigma_{sca\text{-}d,j}$ is the dependent scattering efficiency of the jth sampled observation particle.[42] A derivation of eqs 8 and 9 is presented in section 4 of the Supporting Information.

Figure 5 compares the result of eq 8 to the direct calculations from Figure 4. The comparison was done for fill fractions of 10% and 40% in 88 nm diameter Si films (Figure 5a,b) and in 280 nm diameter GaN films (Figure 5c,d). The results for fill fractions of 20% and 30% are shown in Figure S8. Satisfyingly, we find a good agreement between eq 8 and the results from full-wave calculations. Alternatively, effective medium theories such as the Bruggeman and Maxwell-Garnett mixing formulas did not accurately predict the film's RTA response.

Figure 6 shows the angle- and polarization-dependent RTA responses of both Si and GaN nanoparticle films with 20% fill fraction. The response of the random Si Kerker film is plotted at a wavelength of 420 nm (Figure S9) for backward-Kerker behavior and at 459 nm (Figure 6a) for forward-Kerker scattering. A comparison to the response of an 88 nm thick Si homogeneous dense thin film is shown in Figure 6d. Figure 6b,c,e,f shows the analogous comparisons for GaN. Unlike the thin film cases, we see that the RTA response of the Kerker particle films are relatively unchanged for angles of incidence lower than 40°. At steeper angles, reflection begins to increase and transmission decreases accordingly, while absorption stays relatively constant. This effect is most pronounced at wavelengths with forward-direction Kerker scattering. The RTA response of the random Kerker films are also invariant to incident polarization state and show no Brewster's angle suppression of transverse magnetic reflective. This behavior is completely different to the case of a homogeneous dense thin film.

CONCLUSION

In summary, we show that Kerker scattering achieved by ED and MD overlap in small size parameter particles can create either forward-only scattering or scattering with a backward-to-forward transition as the wavelength is varied. Using 280 nm diameter GaN nanoparticles as an example of forward-only scattering and 88 nm diameter Si nanoparticles as an example of a backward-to-forward scattering transition, we study the effect of random particle coupling in monolayer particle films. The scattering properties of an individual Kerker particles in a random film was weakly affected by particle coupling. In an average sense, the scattering properties mimic the isolated Mie response with the introduction of an added cross-polarization term. This term was roughly an order of magnitude weaker than the dominant terms and had random phase. Random films of Kerker particles had reflection and transmission spectra that could be predicted from three values: the average particle scattering cross-section, the forward-to-backward ratio, and the films area fill fraction. In all cases the spectrum was

https://dx.doi.org/10.1021/acsphotonics.0c00545
ACS Photonics XXXX, XXX, XXX−XXX

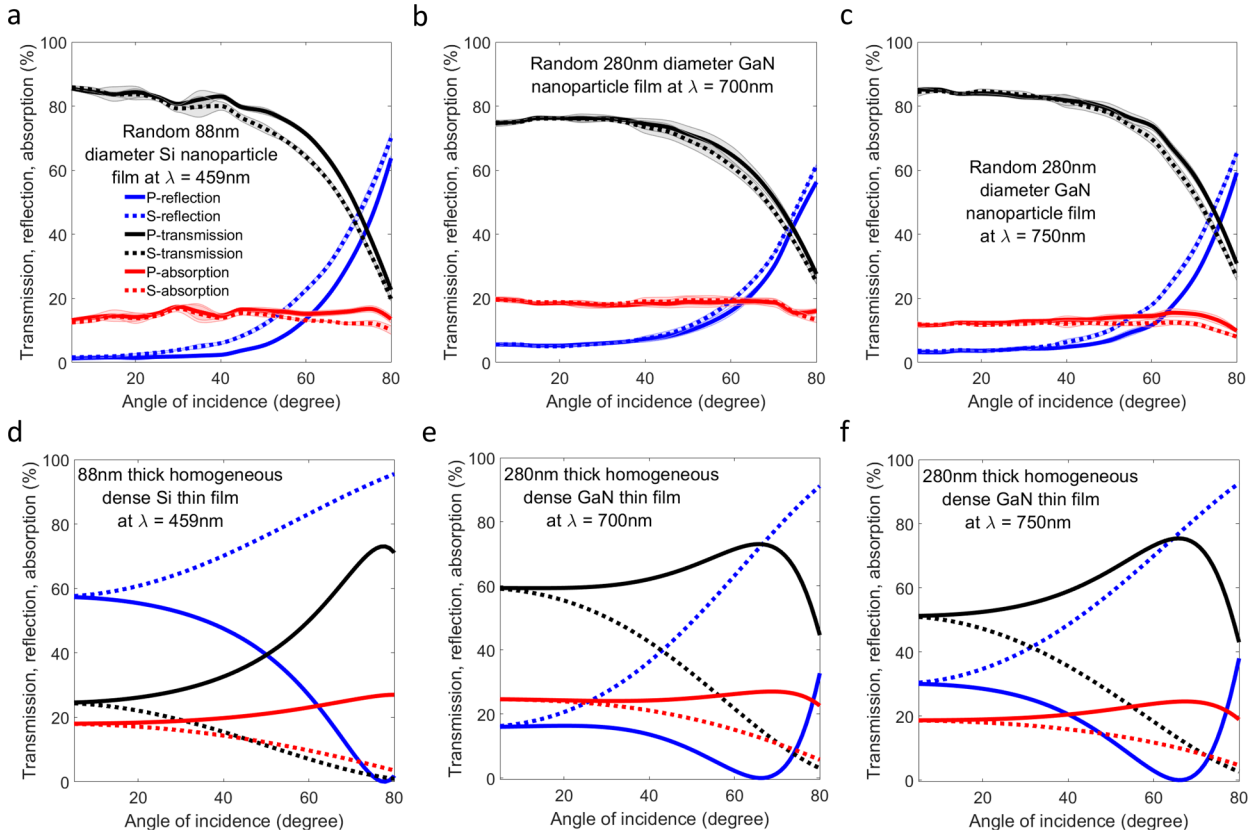

Figure 6. Angular and polarization response of random Kerker films with a fill fraction of 20% and a comparison to equivalent thickness thin film analogs. (a) RTA for randomly placed 88 nm diameter Si particles as a function of angle, at a wavelength of 459 nm (forward-Kerker regime). (b) RTA for randomly placed 280 nm diameter GaN particles as a function of angle, at a wavelength of 700 nm (High-energy end of the forward-Kerker regime). (c) RTA for randomly placed 280 nm diameter GaN particles as a function of angle, at a wavelength of 750 nm (low-energy end of the forward-Kerker regime). (d) Corresponding RTA angular response for an 88 nm thick homogeneous dense Si slab at a wavelength of 459 nm. (e) Corresponding 280 nm thick GaN slab analog at a wavelength of 700 nm. (f) Corresponding 280 nm thick GaN slab analog at a wavelength of 750 nm. For the random films, the particle distributions are the same as the ones used in Figure 4, for the 20% fill fraction case. For a–c, the lines represent the average from the three distinct simulations, and the shaded area represents the area within one standard deviation from the mean. All solid lines represent plane wave excitation with p-polarization. All dashed lines represent s-polarization.

distinctly different from thin-film analogs or effective medium predictions. Finally, we showed that the reflection and transmission response of random Kerker films does not differentiate between s- and p-polarizations and that these films do not exhibit a Brewster angle reflection like that of a thin film sample.

■ ASSOCIATED CONTENT

Supporting Information

The Supporting Information is available free of charge at https://pubs.acs.org/doi/10.1021/acsphotonics.0c00545.

Definition of the scattering amplitude coefficients for an isolated and coupled particle using generalized Mie theory, definition of particle efficiencies in generalized Mie theory, derivation of estimating the RTA response of random films of Kerker particles, regime of higher order mode contributions when designing isolated Kerker particles, the effect of material loss on satisfying Kerker's scattering condition, average autocorrelation of the simulated random particle distributions, higher order mode contributions of coupled Kerker particles in a random film, primary mode contributions of coupled Kerker particles with 20% and 30% area fill fraction, and comparison of RTA response of random Kerker particle films with 20% and 30% area fill fraction (PDF)

■ AUTHOR INFORMATION

Corresponding Author

Harry A. Atwater − *Thomas J. Watson Laboratories of Applied Physics, California Institute of Technology, Pasadena, California 91125, United States;* orcid.org/0000-0001-9435-0201; Email: haa@caltech.edu

Author

Parker R. Wray − *Department of Electrical Engineering, California Institute of Technology, Pasadena, California 91125, United States*

Complete contact information is available at: https://pubs.acs.org/10.1021/acsphotonics.0c00545

Author Contributions

P.R.W. and H.A.A. devised the research idea. P.R.W. performed simulations and interpreted results. H.A.A. oversaw the project progress. Both authors contributed to writing and editing the manuscript.

Notes

The authors declare no competing financial interest.

https://dx.doi.org/10.1021/acsphotonics.0c00545
ACS Photonics XXXX, XXX, XXX−XXX

■ ACKNOWLEDGMENTS

This work was supported by the Army Research Office under MURI Grant W911NF-18-1-0240. We thank M. Su and R. Sokhoyan for commentary and discussions, and also H. Andaraarachchi and N. Uner of the Kortshagen group at U. Minnesota and the Thimsen group at Washington University for useful discussions. This research used the resources of the National Energy Research Scientific Computing Center (NERSC), a U.S. Department of Energy Office of Science User Facility operated under Contract No. DE-AC02-05CH11231.

■ REFERENCES

(1) Kapitanova, P.; Odit, M.; Danaeifar, M.; Sayanskiy, A.; Belov, P.; Miroshnichenko, A.; Kivshar, Y. All-Dielectric Bianisotropic and Multimode Unidirectional Microwave Metasurfaces. *In 2017 47th European Microwave Conference (EuMC)* **2017**, 476−479.

(2) Krasnok, A. E.; Miroshnichenko, A. E.; Belov, P. A.; Kivshar, Y. S. All-Dielectric Optical Nanoantennas. *Opt. Express* **2012**, *20* (18), 20599.

(3) Arslan, D.; Chong, K. E.; Miroshnichenko, A. E.; Choi, D.-Y.; Neshev, D. N.; Pertsch, T.; Kivshar, Y. S.; Staude, I. Angle-Selective All-Dielectric Huygens' Metasurfaces. *J. Phys. D: Appl. Phys.* **2017**, *50* (43), 434002.

(4) Fu, Y. H.; Kuznetsov, A. I.; Miroshnichenko, A. E.; Yu, Y. F.; Luk'yanchuk, B. Directional Visible Light Scattering by Silicon Nanoparticles. *Nat. Commun.* **2013**, *4* (1), 1527.

(5) Geffrin, J. M.; García-Cámara, B.; Gómez-Medina, R.; Albella, P.; Froufe-Pérez, L. S.; Eyraud, C.; Litman, A.; Vaillon, R.; González, F.; Nieto-Vesperinas, M.; Sáenz, J. J.; Moreno, F. Magnetic and Electric Coherence in Forward- and Back-Scattered Electromagnetic Waves by a Single Dielectric Subwavelength Sphere. *Nat. Commun.* **2012**, *3*, 1171.

(6) Limonov, M. F.; Nikulin, A. V.; Li, S. V.; Samusev, K. B.; Kivshar, Y. S.; Rybin, M. V. Mie Bands in All-Dielectric High-Index Metamaterials. In *2017 Progress In Electromagnetics Research Symposium - Spring (PIERS)*, May 22−25, 2017, St. Petersburg, Russia, IEEE, 2017; pp 2825−2827. DOI: 10.1109/PIERS.2017.8262234.

(7) Babicheva, V. E.; Evlyukhin, A. B. Resonant Lattice Kerker Effect in Metasurfaces With Electric and Magnetic Optical Responses. *Laser & Photonics Reviews* **2017**, *11* (6), 1700132.

(8) Kruk, S.; Kivshar, Y. Functional Meta-Optics and Nanophotonics Governed by Mie Resonances. *ACS Photonics* **2017**, *4* (11), 2638−2649.

(9) Person, S.; Jain, M.; Lapin, Z.; Sáenz, J. J.; Wicks, G.; Novotny, L. Demonstration of Zero Optical Backscattering from Single Nanoparticles. *Nano Lett.* **2013**, *13* (4), 1806−1809.

(10) Krasnok, A. E.; Miroshnichenko, A. E.; Belov, P. A.; Kivshar, Yu. S. Huygens Optical Elements and Yagi—Uda Nanoantennas Based on Dielectric Nanoparticles. *JETP Lett.* **2011**, *94* (8), 593−598.

(11) Liu, W.; Kivshar, Y. S. Generalized Kerker Effects in Nanophotonics and Meta-Optics. *Opt. Express* **2018**, *26* (10), 13085.

(12) Yang, Y.; Miroshnichenko, A. E.; Kostinski, S. V.; Odit, M.; Kapitanova, P.; Qiu, M.; Kivshar, Y. S. Multimode Directionality in All-Dielectric Metasurfaces. *Phys. Rev. B: Condens. Matter Mater. Phys.* **2017**, *95* (16), 165426.

(13) Spinelli, P.; Verschuuren, M. A.; Polman, A. Broadband Omnidirectional Antireflection Coating Based on Subwavelength Surface Mie Resonators. *Nat. Commun.* **2012**, *3* (1), 692.

(14) Vaskin, A.; Bohn, J.; Chong, K. E.; Bucher, T.; Zilk, M.; Choi, D.-Y.; Neshev, D. N.; Kivshar, Y. S.; Pertsch, T.; Staude, I. Directional and Spectral Shaping of Light Emission with Mie-Resonant Silicon Nanoantenna Arrays. *ACS Photonics* **2018**, *5* (4), 1359−1364.

(15) Chong, K. E.; Wang, L.; Staude, I.; James, A. R.; Dominguez, J.; Liu, S.; Subramania, G. S.; Decker, M.; Neshev, D. N.; Brener, I.; Kivshar, Y. S. Efficient Polarization-Insensitive Complex Wavefront Control Using Huygens' Metasurfaces Based on Dielectric Resonant Meta-Atoms. *ACS Photonics* **2016**, *3* (4), 514−519.

(16) Abdelrahman, M. I.; Saleh, H.; Fernandez-Corbaton, I.; Gralak, B.; Geffrin, J.-M.; Rockstuhl, C. Experimental Demonstration of Spectrally Broadband Huygens Sources Using Low-Index Spheres. *APL Photonics* **2019**, *4* (2), 020802.

(17) Shamkhi, H. K.; Sayanskiy, A.; Valero, A. C.; Kupriianov, A. S.; Kapitanova, P.; Kivshar, Y. S.; Shalin, A. S.; Tuz, V. R. Invisibility and Perfect Absorption of All-Dielectric Metasurfaces Originated from the Transverse Kerker Effect. *Phys. Rev. Mater.* **32019**085201.

(18) Born, M.; Wolf, E. *Principles of Optics: Electromagnetic Theory of Propagation, Interference and Diffraction of Light*; Pergamon Press, 2000.

(19) Kerker, M.; Wang, D.-S.; Giles, C. L. Electromagnetic Scattering by Magnetic Spheres. *J. Opt. Soc. Am.* **1983**, *73* (6), 765.

(20) Lannebère, S.; Campione, S.; Aradian, A.; Albani, M.; Capolino, F. Artificial Magnetism at Terahertz Frequencies from Three-Dimensional Lattices of TiO_2 Microspheres Accounting for Spatial Dispersion and Magnetoelectric Coupling. *J. Opt. Soc. Am. B* **2014**, *31* (5), 1078.

(21) Paniagua-Domínguez, R.; Yu, Y. F.; Miroshnichenko, A. E.; Krivitsky, L. A.; Fu, Y. H.; Valuckas, V.; Gonzaga, L.; Toh, Y. T.; Kay, A. Y. S.; Luk'yanchuk, B.; Kuznetsov, A. I. Generalized Brewster Effect in Dielectric Metasurfaces. *Nat. Commun.* **2016**, *7* (1), 10362.

(22) Evlyukhin, A. B.; Novikov, S. M.; Zywietz, U.; Eriksen, R. L.; Reinhardt, C.; Bozhevolnyi, S. I.; Chichkov, B. N. Demonstration of Magnetic Dipole Resonances of Dielectric Nanospheres in the Visible Region. *Nano Lett.* **2012**, *12* (7), 3749−3755.

(23) Liu, W.; Zhang, J.; Lei, B.; Ma, H.; Xie, W.; Hu, H. Ultra-Directional Forward Scattering by Individual Core-Shell Nanoparticles. *Opt. Express* **2014**, *22* (13), 16178.

(24) Hopkins, B.; Filonov, D. S.; Miroshnichenko, A. E.; Monticone, F.; Alù, A.; Kivshar, Y. S. Interplay of Magnetic Responses in All-Dielectric Oligomers To Realize Magnetic Fano Resonances. *ACS Photonics* **2015**, *2* (6), 724−729.

(25) Miroshnichenko, A. E.; Kivshar, Y. S. Fano Resonances in All-Dielectric Oligomers. *Nano Lett.* **2012**, *12* (12), 6459−6463.

(26) Yan, J. H.; Liu, P.; Lin, Z. Y.; Wang, H.; Chen, H. J.; Wang, C. X.; Yang, G. W. Magnetically Induced Forward Scattering at Visible Wavelengths in Silicon Nanosphere Oligomers. *Nat. Commun.* **2015**, *6*, 7042.

(27) Vasilantonakis, N.; Scheuer, J.; Boag, A. Designing High-Transmission and Wide Angle All-Dielectric Flat Metasurfaces at Telecom Wavelengths. *arXiv:1711.01430 [physics]* **2017**, na.

(28) Yang, Y.; Kravchenko, I. I.; Briggs, D. P.; Valentine, J. All-Dielectric Metasurface Analogue of Electromagnetically Induced Transparency. *Nat. Commun.* **2014**, *5* (1), 5753.

(29) Yang, T.; Wang, X.; Zhou, Z.; Zhou, J. Transient Characters of the Unity Reflection Phenomenon in All-Dielectric Magnetic Metamaterials. *OSA Continuum* **2018**, *1* (2), 634.

(30) Moitra, P.; Slovick, B. A.; Li, W.; Kravchencko, I. I.; Briggs, D. P.; Krishnamurthy, S.; Valentine, J. Large-Scale All-Dielectric Metamaterial Perfect Reflectors. *ACS Photonics* **2015**, *2* (6), 692−698.

(31) Ra'di, Y.; Asadchy, V. S.; Kosulnikov, S. U.; Omelyanovich, M. M.; Morits, D.; Osipov, A. V.; Simovski, C. R.; Tretyakov, S. A. Full Light Absorption in Single Arrays of Spherical Nanoparticles. *ACS Photonics* **2015**, *2* (5), 653−660.

(32) Bohren, C. F.; Huffman, D. R. *Absorption and Scattering of Light by Small Particles*; Wiley-VCH: Weinheim, 2004.

(33) Aspnes, D. E.; Studna, A. A. Dielectric Functions and Optical Parameters of Si, Ge, GaP, GaAs, GaSb, InP, InAs, and InSb from 1.5 to 6.0 EV. *Phys. Rev. B: Condens. Matter Mater. Phys.* **1983**, *27* (2), 985−1009.

(34) Kawashima, T.; Yoshikawa, H.; Adachi, S.; Fuke, S.; Ohtsuka, K. Optical Properties of Hexagonal GaN. *J. Appl. Phys.* **1997**, *82* (7), 3528−3535.

(35) Mätzler, C. MATLAB Functions for Mie Scattering and Absorption.. *Research Report No. 2002-08*; Institut fur Angewandte Physik, 2002.

https://dx.doi.org/10.1021/acsphotonics.0c00545
ACS Photonics XXXX, XXX, XXX−XXX

(36) Ziolkowski, R. W. Using Huygens Multipole Arrays to Realize Unidirectional Needle-Like Radiation. *Phys. Rev. X* **2017**, *7* (3), na DOI: 10.1103/PhysRevX.7.031017.
(37) Babicheva, V. E.; Evlyukhin, A. B. Resonant Lattice Kerker Effect in Metasurfaces With Electric and Magnetic Optical Responses. *Laser & Photonics Reviews* **2017**, *11* (6), 1700132.
(38) Babicheva, V. E.; Evlyukhin, A. B. Metasurfaces with Electric Quadrupole and Magnetic Dipole Resonant Coupling. *ACS Photonics* **2018**, *5* (5), 2022−2033.
(39) Mackowski, D. W.; Mishchenko, M. I. Calculation of the T Matrix and the Scattering Matrix for Ensembles of Spheres. *J. Opt. Soc. Am. A* **1996**, *13* (11), 2266.
(40) Mackowski, D. W.; Mishchenko, M. I. A Multiple Sphere T-Matrix Fortran Code for Use on Parallel Computer Clusters. *J. Quant. Spectrosc. Radiat. Transfer* **2011**, *112* (13), 2182−2192.
(41) Lumerical Inc. https://www.Lumerical.Com/Products/.
(42) Mackowski, D. W.; Mishchenko, M. I. A Multiple Sphere T-Matrix FORTRAN Code for Use on Parallel Computer Clusters. *J. Quant. Spectrosc. Radiat. Transfer* **2011**, *112*, 2182−2192.

https://dx.doi.org/10.1021/acsphotonics.0c00545
ACS Photonics XXXX, XXX, XXX−XXX